Supporting Information for

Biophysical Examination of the Calcium-Modulated Nickel-Binding Properties of Human Calprotectin Reveals Conformational Change in the EF-Hand Domains and His_3Asp Site

Toshiki G. Nakashige,[1] Sarah E. J. Bowman,[1,2,3,4] Emily M. Zygiel,[1] Catherine L. Drennan,[1,2,3,*] and Elizabeth M. Nolan[1,*]

[1]Department of Chemistry, [2]Department of Biology, and [3]Howard Hughes Medical Institute, Massachusetts Institute of Technology, Cambridge, MA 02139, USA

[4]Current address: Hauptman-Woodward Medical Research Institute, Buffalo, NY 14203, USA

*Corresponding authors: cdrennan@mit.edu and lnolan@mit.edu

Phone: 617-452-2495

This Supporting Information includes:

Experimental Methods

Materials and General Methods. All chemicals were obtained from commercial suppliers and used as received unless otherwise noted. All aqueous solutions and media were prepared using Milli-Q water (18.2 MΩ•cm, 0.22-μm filter). Buffers were prepared with Ultrol grade HEPES (Calbiochem), TraceSELECT NaCl (Sigma), and TraceSELECT NaOH (Sigma) in either acid-washed volumetric glassware or polypropylene containers, using disposable plastic spatulas or polypropylene pipettes. Stock solutions of metal ions were prepared in acid-washed volumetric glassware by dissolving 99.99% $CaCl_2$ (1.0 M), 99.99% $NiCl_2$ (1.0 M), and 99.999% anhydrous $ZnCl_2$ (100 mM) (Sigma) into water. Working metal stock solutions were prepared by serial dilution immediately before each experiment and stored in polypropylene containers. Crystallization solutions were prepared from reagents and solutions purchased from Hampton Research. Zinpyr-1 (ZP1) was synthesized from 2′,7′-dichlorofluorescein and di(2-picolyl)amine as described.[1] Stock solutions of 2 mM ZP1 (≈15 μL) were prepared in dimethyl sulfoxide (DMSO, Sigma) and were stored at −20 °C. All ZP1 solutions were handled in the dark. All protein variants were overexpressed and purified as described previously.[2-3] CP variants employed in this work are based on CP-Ser (Table 1). CP-Ser is the heterooligomer of S100A8(C3S) and S100A9(C42S), and this variant has comparable antimicrobial activity to native CP. The biotinylated CP variant B-ΔHis$_3$Asp was prepared as described previously.[4] Protein stocks were thawed only once immediately prior to use.

Crystallization of Ni(II)-bound CP-Ser. Initial crystallization conditions were identified by crystallization screens using a Phoenix Liquid Handling System (Art Robbins Instrument). Larger Ni(II)-bound CP-Ser crystals were subsequently obtained by optimizing the initial crystallization conditions and employing sitting-drop vapor-diffusion technique at room temperature using 24-well crystallization plates (Hampton Research). CP-Ser was buffer exchanged in 75 mM HEPES,

100 mM NaCl, pH 7.0 using 10K MWCO Amicon spin filters (Millipore), and a 100-μL solution of 100 μM CP-Ser (2.4 mg/mL) and 100 μM Ni(II) (added from a 100-mM $NiCl_2$ stock solution) was prepared in buffer. A precipitant solution containing 200 mM Li_2SO_4, 100 mM Tris, 20% (v/v) PEG 3350, pH 8.0 was prepared. To each crystallization well, 1 μL of the protein sample and 1 μL of precipitant solution was added. The drop was allowed equilibrate against 500 μL of precipitant solution. Protein crystals formed in an orthorhombic $P2_12_12_1$ space group within 3 to 5 days. A cryogenic solution containing 200 mM Li_2SO_4, 100 mM Tris, 30% (v/v) PEG 3350, 10% (v/v) PEG 200, pH 8.0 was prepared. The crystals were transferred to a 2-μL drop of the cryogenic solution using a 100-μm loop, allowed to equilibrate for ≈10 s, and flash frozen in liquid nitrogen.

Energy Dispersive X-ray Spectroscopy. Energy dispersive X-ray (EDX) spectroscopy was performed on each crystal prior to X-ray diffraction data collection. Emission line scans were acquired at a fixed incident energy 0.9792 Å (12,622 eV) by measuring fluorescence counts using an Amptek X-123SDD Silicon Drift Diode (SDD) detector on beamline 24ID-C at the Advanced Photon Source (APS) at the Argonne National Laboratory (Illinois, USA). The fluorescence counts were binned into 4,096 channels on the SDD, which were calibrated and converted to energy units using known elements: samarium (L-edge transitions $L\alpha_1$ 5.64 eV, $L\beta_1$ 6.21 keV), nickel (K-edge transitions $K\alpha_1$ 7.48 keV, $K\beta_1$ 8.26 keV), zinc ($K\alpha_1$ 8.64 keV, $K\beta_1$ 9.57 keV), bromine ($K\alpha_1$ 11.92 keV, $K\beta_1$ 13.29 keV), and strontium ($K\alpha_1$ 14.16 keV, $K\beta_1$ 15.83 keV). The Amptek SDD detector has an energy resolution of ca. 130 eV. DppMCA Digital Acquisition Software (Version 1.0.0.16, Amptek) was used to collect the experimental and calibration data. R Statistical Software was used to analyze the data.[5]

Data Collection, Processing, and Structure Determination of Ni(II)-bound CP-Ser. All X-ray diffraction data were collected at beamline 24ID-C at the APS using a Pilatus 6M pixel detector at in 0.25º oscillation steps at 100 K (Table S2). Native datasets were collected at 0.9792 Å (12,622 eV). Ni anomalous datasets were collected at 1.4831 Å (8,360 eV). Fe anomalous

datasets were collected at 1.7370 Å (7,138 eV). SBGrid software[6] was employed to complete the structures. Data were processed in HKL2000.[7] The structure of Ni(II)-bound CP-Ser was determined to 2.1-Å resolution by molecular replacement using the protein atoms of chains A and B of Mn(II)-, Ca(II)-, and Na(I)-bound CP-Ser (PDB: 4XJK)[8] in Phaser.[9] The asymmetric unit contains two $\alpha_2\beta_2$ heterotetramers. The structures were completed by iterative refinement in PHENIX[10] employing two-fold noncrystallographic symmetry and model building in COOT.[11] The Ni and Fe anomalous scattering datasets were processed using HKL2000, and anomalous density maps were generated in PHENIX.

Protein residues were modeled first during structure refinement. Metal ions and water molecules were subsequently added. Composite omit maps were used to validate the structure. The presence of Ni(II) ions were determined by employing the Ni anomalous data. In the final model, Ni(II) ions were modeled in at 100% occupancy. Na(I) ions were modeled at the EF-hand domains. Na(I) ions refined with no difference electron density, whereas refinement with Ca(II) ions resulted in negative difference electron density. Negligible anomalous scattering at the Fe peak was observed in the structure, supporting the absence of Ca(II) ions at the EF-hand domains. No distance or angle restraints were used in the refinement of the metal sites. No difference in metal speciation was observed between the two heterotetramers in the asymmetric unit. The final model of the Ni(II)-bound CP-Ser $\alpha_2\beta_2$ heterotetramer comprises of residues 1–89 for chain A (93 residues total), residues 4–111 for chain B (114 residues total), residues 1–89 for chain C (93 residues total), and residues 5–112 (114 residues total).

Analytical Size-Exclusion Chromatography. Analytical size-exclusion chromatography (SEC) was performed employing an ÄKTA purifier with a Superdex 75 10/300 GL column (GE Healthcare Life Sciences) housed at 4 ºC. The calibration of the column using a low-molecular-weight calibration kit (GE Healthcare Life Sciences) as described previously.[2] Protein solutions were buffer exchanged into 75 mM HEPES, 100 mM NaCl, pH 7.0 buffer. Samples (20 μM, 300

μL) were loaded into a 100-μL loop, and to ensure that the total volume in the loop was transferred to the column, a 500-μL volume was injected. The protein was eluted over 1 column volume of running buffer (75 mM HEPES, 100 mM NaCl, pH 7.0). For conditions containing Ni(II), the protein samples were pre-incubated with 5 equiv Ni(II). For samples containing Ca(II), the running buffer contained 2 mM Ca(II). To compare peak elution volumes, the chromatograms were normalized to maximum peak heights of 1.

Circular Dichroism Spectroscopy and Thermal Denaturation. An Aviv Model 202 Circular Dichroism (CD) spectrometer was employed for CD spectroscopy. A thin-walled Hellma quartz cuvette was washed with 300 μM ethylenediaminetetraacetic acid (EDTA, Sigma), 20% HNO_3 (prepared from trace metals basis concentrated HNO_3, Sigma), and Milli-Q water. Protein samples (10 μM, 300 μL) were prepared in Chelex-treated 1.0 mM Tris-HCl, pH 7.5 buffer. For samples with Ni(II), 5 equiv Ni(II) was added from a 1-mM stock solution, and for samples with Ca(II), 2 mM Ca(II) was added from a 100-mM stock solution. CD spectra were collected from 260 to 195 nm (3 independent scans per wavelength, 3 s averaging time, 1 nm step). For routine CD measurements, the spectrometer was maintained at 25 ºC. For the thermal denaturation experiments, the temperature was increased from 25 to 95 ºC in 2-ºC intervals (1 min equilibration time, 3 s averaging time at each temperature), and the ellipticity at 222 nm was monitored. The temperature scan data were plotted in Excel, normalizing the lowest ellipticity value as 0% unfolded protein and the highest ellipticity value as 100% unfolded protein, and the melting temperature was measured from these plots.

Ni(II) Competition Experiments. Fluorescence spectroscopy was performed using a Photon Technologies International QuantaMaster 40 fluorometer outfitted with a continuous xenon source for excitation, autocalibrated QuadraScopic monochromators, a multimode PMT detector and a circulating water bath maintained at 25 ºC. Spectra were recorded and integrated using the FelixGX software package. Quartz cuvettes with 1-cm path lengths (Starna) were

employed, and were thoroughly washed with 20% HNO_3 and Milli-Q water before use. The excitation wavelength was 490 nm. The emission was measured from 500 to 650 nm at a scan rate of 10 nm/s. The excitation and emission slit widths were set to 1.6 nm.

The competition for Ni(II) between ZP1 and CP variants in the absence and presence of Ca(II) was examined. In each cuvette, a 2-mL solution of 1 μM ZP1 was prepared in 75 mM HEPES, 100 mM NaCl, pH 7.0. Protein stocks were buffer exchanged into 75 mM HEPES, 100 mM NaCl, pH 7.0 using 10K MWCO Amicon spin concentrators (Millipore), and 4 μM protein was added to the cuvette. From a 100-mM stock solution of Ca(II), 200 μM Ca(II) was added. The mixture was allowed to equilibrate for ≈30 min at room temperature. The emission of each sample was measured. To each sample, 2 μM Ni(II) from a 1-mM stock solution was added. The cuvettes were covered with Parafilm to limit evaporation, and the samples were incubated at room temperature for 20 h. The emission spectra were measured at this time point. "ZP1 only" samples without protein in the absence and presence of Ca(II) were also prepared and analyzed. For each measurement, the integrated emission from 500 to 650 nm was normalized to that of the Ni(II)-free sample. Three independent trials were conducted, and the mean and SDM are reported (*n* = 3).

Metal Substitution Assay: Site 2. To evaluate the effect of Ca(II) on the exchange between Ni(II) and Zn(II) at site 2, a metal substitution time course experiment was performed by modifying a biotin pull-down assay described previously.[4] Protein solutions were buffer exchanged into 75 mM HEPES, 100 mM NaCl, pH 7.0 buffer. Samples (3 mL) with 10 μM B-ΔHis_3Asp were prepared in the absence and presence of 2 mM Ca(II) in 75 mM HEPES, 100 mM NaCl, pH 7.0 in 5-mL centrifuge tubes. To each sample, 10 μM Ni(II) or Zn(II) was added. After the solution equilibrated for 30 min at room temperature, 10 μM of the second metal was added to each sample (i.e., Zn(II) in the Ni(II)-bound B-ΔHis_3Asp sample, Ni(II) in the Zn(II)-bound B-ΔHis_3Asp sample). The samples were incubated at room temperature. At t = 4, 8, 24, 48, and 72

h, a 500-μL portion of the protein mixture was treated with high capacity streptavidin agarose resin (Pierce, Thermo Scientific). Resin (150 μL) was washed three times in a 1.7-mL microcentrifuge tube with 500 μL buffer (75 mM HEPES, 100 mM NaCl, pH 7.0) by centrifuging (13,000 rpm, 3 min, 4 ºC), removing the supernatant, and resuspending with fresh buffer. After a final centrifugation step, the buffer supernatant was removed, and 500 μL of the metal/protein sample was transferred from the 5-mL centrifuge tube to the resin. The resin mixture was mixed by inverting and allowed to equilibrate for 30 min on a rocking platform at room temperature. The resin was pelleted by centrifugation, and 400 μL of the remaining solution without B-ΔHis_3Asp were transferred to 15-mL Falcon tubes with 1.6 mL of 3% HNO_3, 100 μL of concentrated HNO_3, and 40 μL of 1 ppb terbium (Tb, serially diluted from a 10-ppm Agilent standard solution).

Metal analysis on each supernatant sample was performed by inductively coupled plasma-mass spectrometry using an Agilent 7900 ICP-MS in helium mode outfitted with an integrated autosampler. The instrument was calibrated using standards prepared by serial dilution of the Agilent Environmental Calibration Standard solution. The concentrations of Mg, Ca, Mn, Fe, Co, Ni, Cu, and Zn were quantified, and Tb was used as an internal standard. Four independent trials were conducted using at least two different protein preparations. The mean metal concentration values and SDM are reported (n = 4).

Metal Substitution Assay: Site 1. To evaluate the preference for Ni(II) or Zn(II) at site 1, a metal substitution time course experiment was performed using spin filtration to separate protein-bound and unbound metal. Protein solutions were buffer exchanged into 75 mM HEPES, 100 mM NaCl, pH 7.0. Samples (10 mL) of 10 μM CP-Ser or ΔHis_3Asp were prepared in the absence or presence of 2 mM Ca(II) in 75 mM HEPES, 100 mM NaCl, pH 7.0 in 15-mL Falcon tubes. To each sample, 20 μM Ni(II) (CP-Ser) or 10 μM Ni(II) (ΔHis_3Asp) was added from a 10-mM stock solution in 75 mM HEPES, 100 mM NaCl, pH 7.0. After the protein solutions were allowed to equilibrate for 1 h at room temperature, 10 μM of Zn(II) was added to each protein

solution from a 10 mM stock in 75 mM HEPES, 100 mM NaCl, pH 7.0. The samples were incubated at room temperature or 37 °C on a nutating platform. At t = 0, 10, 20, 40, 60, and 120 min, a 1-mL portion of each protein solution was applied to a 4-mL 10K MWCO spin filter (Millipore) and centrifuged for 10 min at 3750 rpm, 4 °C. The t = 0 aliquot was taken before $ZnCl_2$ addition. Filtrate (500 μL) was diluted into 1.5 mL of 5% HNO_3 in 15-mL Falcon tubes and supplemented with 1 ppb Tb. Metal analysis was performed as described above for metal substitution at site 2. The mean metal concentration values and SDM are reported (*n* = 3).

Supporting Discussion

For the studies of metal substitution at the His_3Asp site of CP-Ser, several different assay protocols were evaluated that involved the ΔHis_4 variant and proved to be problematic. As described in the main text, only low yields were achieved when we biotinylated the ΔHis_4 variant at the Cys3 position of the S100A9 subunit. We then considered a filtration-based approach in which the ΔHis_4 variant was incubated with 1.0 equiv Ni(II) and 1.0 equiv Zn(II) (75 mM HEPES, 100 mM NaCl, pH 7.4) and the bound and unbound fractions were separated via spin filtration (10K MWCO), and the filtrate (unbound fraction) was analyzed by ICP-MS. This setup was also problematic because the ΔHis_4 variant consistently depleted >1.0 equiv of added metal, which we attributed to non-specific binding. Indeed, when we then performed the same protocol in a metal-depleted microbial growth medium that was supplemented with 1.0 equiv of Ni(II) and 1.0 equiv of Zn(II), which contains many competing ligands that can weakly associate with metals in solution, stoichiometric metal depletion occurred. As a result, we decided to employ Ni(II)-bound CP-Ser where the protein was pre-incubated with two equivalents of Ni(II) as described in the main text.

SupportingTables and Figures

Table S1. Nomenclature of Human Calprotectin Variants

Protein	S100A8 Mutation(s)	S100A9 Mutation(s)
CP	N/A	N/A
CP-Ser	C42S	C3S
B-ΔHis_3Asp [a]	C42S, H83A, H87A	H20A, D30A
CP-Ser ΔHis_3Asp	C42S, H83A, H87A	C3S, H20A, D30A
CP-Ser ΔHis_4	C42S, H17A, H27A	C3S, H91A, H95A
CP-Ser $\Delta\Delta$	C42S, H17A, H27A, H83A, H87A	C3S, H20A, D30A, H91A, H95A
CP-Ser(H103A)	C42S	C3S, H103A
CP-Ser(H104A)	C42S	C3S, H104A
CP-Ser(H105A)	C42S	C3S, H105A
CP-Ser-AHA	C42S	C3S, H103A, H105A
CP-Ser-AAA	C42S	C3S, H103A, H104A, H105A

[a] Cys3 of the S100A9 subunit was biotinylated. The preparation of B-ΔHis_3Asp is described previously.[4]

Table S2. Crystallographic Data Collection and Refinement Statistics of Ni(II)-Bound CP-Ser

	Ni(II)-bound CP-Ser		
Data collection			
Wavelength (Å)	0.9792	1.4831 [a]	1.7370 [a]
Space group	$P2_12_12_1$	$P2_12_12_1$	$P2_12_12_1$
Cell dimensions			
a, *b*, *c* (Å)	57.1, 78.1, 223.8	57.1, 78.1, 223.8	57.1, 78.1, 223.8
α, β, γ (°)	90, 90, 90	90, 90, 90	90, 90, 90
Resolution (Å)	46.11–2.10 (2.15–2.10)	50.00–2.30 (2.34–2.30)	50.00–2.60 (2.64–2.60)
No. unique reflections	59476 (5815)	45759 (2213)	31417 (1479)
$CC_{1/2}$	(0.918)	(0.853)	(0.854)
R_{sym} [b]	0.069 (0.448)	0.126 (0.751)	0.146 (0.592)
R_{meas} [b]	0.075 (0.487)	0.133 (0.799)	0.155 (0.642)
$\langle I \rangle / \sigma (\langle I \rangle)$ [b]	26.1 (4.4)	15.2 (4.1)	13.4 (3.3)
Redundancy [b]	6.5 (6.4)	9.1 (8.5)	9.0 (6.3)
Completeness [b]	99.9 (99.7)	99.6 (99.8)	99.3 (99.1)
Refinement			
Resolution (Å)	50.00–2.10		
R_{cryst}/R_{free}	0.1855/0.2219		
No. atoms			
Protein	6603		
Ni/Na	6/10		
H_2O	598		
B-factors (Å^2)			
Protein	27.72		
Solvent	46.25		
Ni	32.56		
Na	32.45		
R.M.S. deviations			
Bond lengths (Å)	0.003		
Bond angles (°)	0.52		
Rotamer outliers (%)	1.65		
Ramachandran			
Outliers (%)	0		
Allowed (%)	1.04		
Favored (%)	98.96		

[a] The Ni anomalous dataset was processed with "Scale Anomalous" in HKL2000. [b] Values in parentheses are for highest-resolution shell.

Table S3. Ni–Ligand Bond Distances at the His_3Asp (Site 1) [a]

Ligand	Ni–Ligand Bond Distance (Å)
Nε2, (A8)His83	2.2 (0.0)
Nε2, (A8)His87	2.0 (0.1)
Nε2, (A9)His20	2.2 (0.0)
Oδ1, (A9)Asp30	2.0 (0.1)
Oδ2, (A9)Asp30	2.6 (0.4)
H_2O	2.5 (0.1)

[a] Average (standard deviation) bond distances for both heterotetramers in the asymmetric unit are shown.

Table S4. Ligand–Ni(II)–Ligand Bond Angles at the His_3Asp Motif (Site 1) [a]

Ligand	Nε2, His83	Nε2, His87	Nε2, His20	Oδ1, Asp30	Oδ2, Asp30	H_2O
Nε2, His83	N/A	95 (8)	94 (2)	93 (4)	88 (4)	167 (2)
Nε2, His87	–	N/A	97 (4)	147 (4)	95 (6)	93 (2)
Nε2, His20	–	–	N/A	113 (6)	167 (1)	89 (0)
Oδ1, Asp30	–	–	–	N/A	55 (8)	74 (4)
Oδ2, Asp30	–	–	–	–	N/A	87 (5)
H_2O	–	–	–	–	–	N/A

[a] Average (standard deviation) bond angles for both heterotetramers in the asymmetric unit are shown.

Table S5. Ni(II)–Ligand Bond Distances at the His_6 Motif (Site 2) [a]

Ligand	Ni–Ligand Bond Distance (Å)
Nε2, (A8)His17	2.3 (0.1)
Nε2, (A8)His27	2.2 (0.1)
Nε2, (A9)His91	2.3 (0.0)
Nε2, (A9)His95	2.2 (0.1)
Nε2, (A9)His103	2.2 (0.1)
Nε2, (A9)His105	2.2 (0.1)

[a] Average (standard deviation) bond distances for both heterotetramers in the asymmetric unit are shown.

Table S6. Ligand–Ni(II)–Ligand Bond Angles at the His_6 Motif (Site 2) [a]

Ligand	Nε2, His17	Nε2, His27	Nε2, His91	Nε2, His95	Nε2, His103	Nε2, His105
Nε2, His17	N/A	96 (1)	88 (1)	174 (2)	87 (1)	87 (3)
Nε2, His27	–	N/A	91 (2)	89 (3)	95 (2)	176 (2)
Nε2, His91	–	–	N/A	88 (1)	173 (3)	91 (3)
Nε2, His95	–	–	–	N/A	93 (5)	89 (1)
Nε2, His103	–	–	–	–	N/A	86 (8)
Nε2, His105	–	–	–	–	–	N/A

[a] Average (standard deviation) bond angles for both heterotetramers in the asymmetric unit are shown.

Table S7. Metal-Binding Ligands at the EF-hand Domains of CP

EF-hand Domain	Ligands
S100A8 N-terminal	C=O, Ser20
	C=O, Lys23
	C=O, Asn25
	C=O, Ala28
	H_2O
S100A8 C-terminal	Oδ1, Asp59
	Oδ1, Asn61
	Oδ1, Asp63
	C=O, Ala65
	Oε1, Glu70
	Oε2, Glu70
	H_2O
S100A9 N-terminal	C=O, Ser23
	C=O, Leu26
	C=O, His28
	C=O, Thr31
	Oε1, Glu36 [a]
	Oε2, Glu36 [a]
	H_2O
	H_2O [b]
S100A9 C-terminal	Oδ1, Asp67
	Oδ1, Asn69
	Oδ1, Asp71
	C=O, Gln73
	Oε1, Glu78
	Oε2, Glu78
	H_2O

[a] In the Ca(II)-bound structures, Glu36 coordinates the metal at the S100A9 N-terminal EF-hand domain. This residue side chain is pointed away from the metal in the Ca(II)-free structure. [b] In the Ca(II)-free structure, a second H_2O molecule coordinates the metal at this site.

Table S8. Protein Ni(II)-Binding Sites [a]

Protein (Reference)	Ligands	CN
NikA (12)	2 His	6
Methyl coenzyme M reductase (13)	1 Ni-tetrapyrrole, 1 coenzyme M, 1 Gln	6
Acireductone dioxygenase (14)	3 His, 1 Glu, 2 H_2O	6
Glyoxylase I (15)	2 His, 2 Glu, 2 H_2O	6
Ni(II)-bound transcriptional regulator TM1602 (16)	3 His, 1 bidentate Glu, 1 H_2O	6
Ni(II)-substituted Zn(II) endopeptidase astacin (17)	3 His, 1 Tyr, 2 H_2O	6
Ni(II)-substituted amine oxidase (18)	3 His, 3 H_2O	6
Ni(II)-substituted phosphoglucose isomerase (19)	3 His, 1 Glu, 2 H_2O	6
Ni(II)-substituted ornithine transcarbamylase (20)	3 His, 3 H_2O	6
Ni(II)-bound YfiT (21)	3 His, 3 H_2O	6
Urease (22)	2 His, 2 H_2O, 1 lysine carbamate; 2 His, 2 H_2O, 1 Asp, 1 lysine carbamate	5/6
UreE (23)	5 His	5
Ni superoxide dismutase (24)	1 terminal amine, 1 backbone amide, 1 His, 2 Cys	5
[NiFe]-hydrogenase (25)	4 Cys, 1 H_2O	5
NikR (26)	3 His, 1 Cys	4
Lactate racemase LarA (27)	1 His, 1 pyridinium-3-thioamide-5-thiocarboxylic acid mononucleotide	4
NikM (26)	ATCUN motif derived from Met1 and 2 His	4
Engineered trypsin N143H, E151H (28)	3 His, 1 H_2O	4
DNA- and Ni(II)-bound ColE7 (29)	3 His, 1 PO_4^{3-}	4
C-terminal regulatory domain of NikR (30)	3 His, 1 Cys	4

[a] The proteins listed in this table have been crystallographically characterized. Proteins that contain Ni as part of a metallocluster are not included.

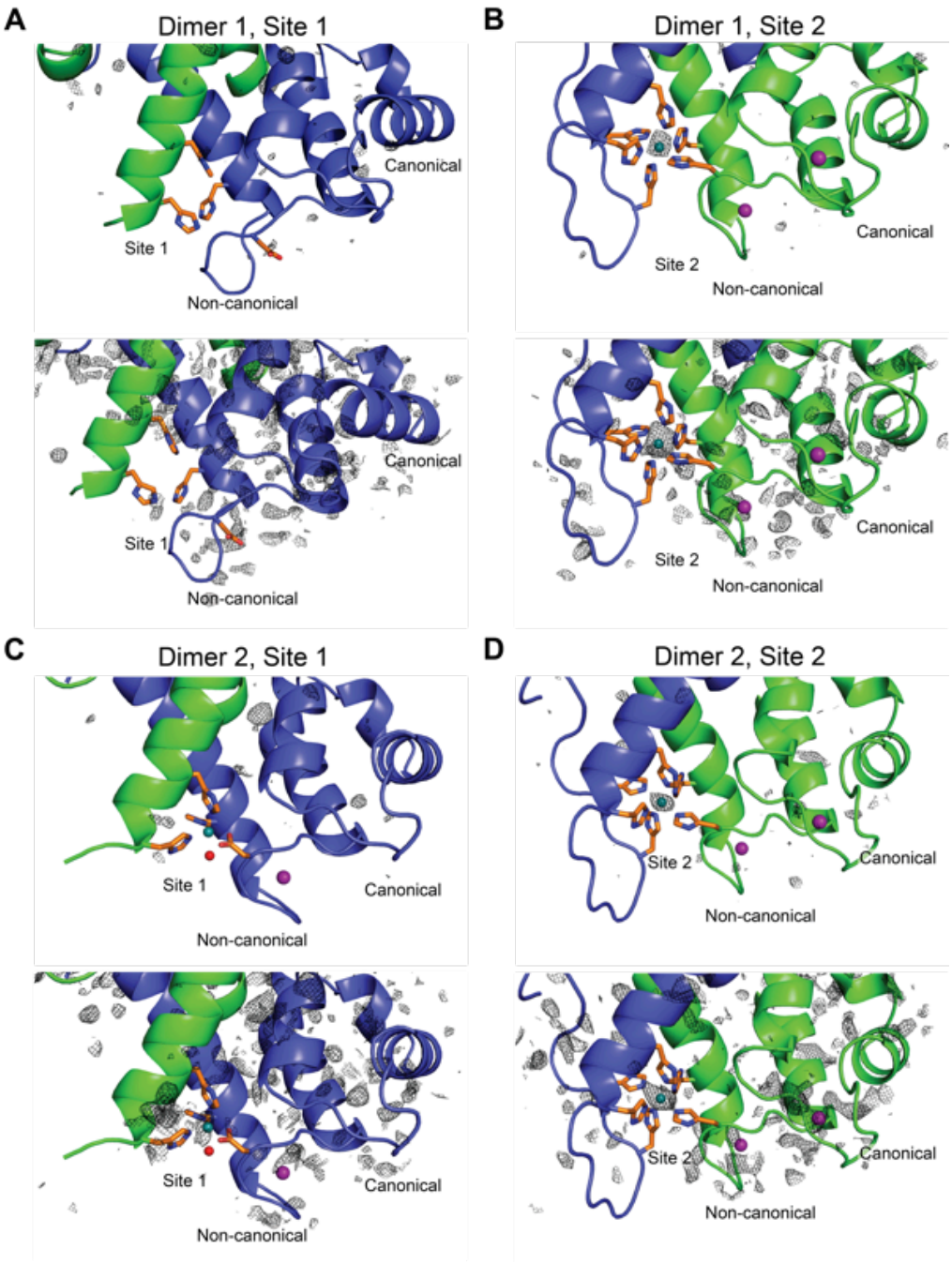

Figure S1. Fe anomalous scattering map. (A) Site 1 and the EF-hand domains of S100A9. (B) Site 2 and the EF-hand domains of S100A8. (C) Site 1 and the EF-hand domains of S100A9. (D) Site 2 and the EF-hand domains of S100A8. The Fe anomalous scattering map generated using data collected at 1.7370 Å is contoured at 3σ (top panels) or 2σ (bottom panels) and is shown in black. S100A8 is green. S100A9 is blue. Ni(II) ions are depicted as teal spheres.

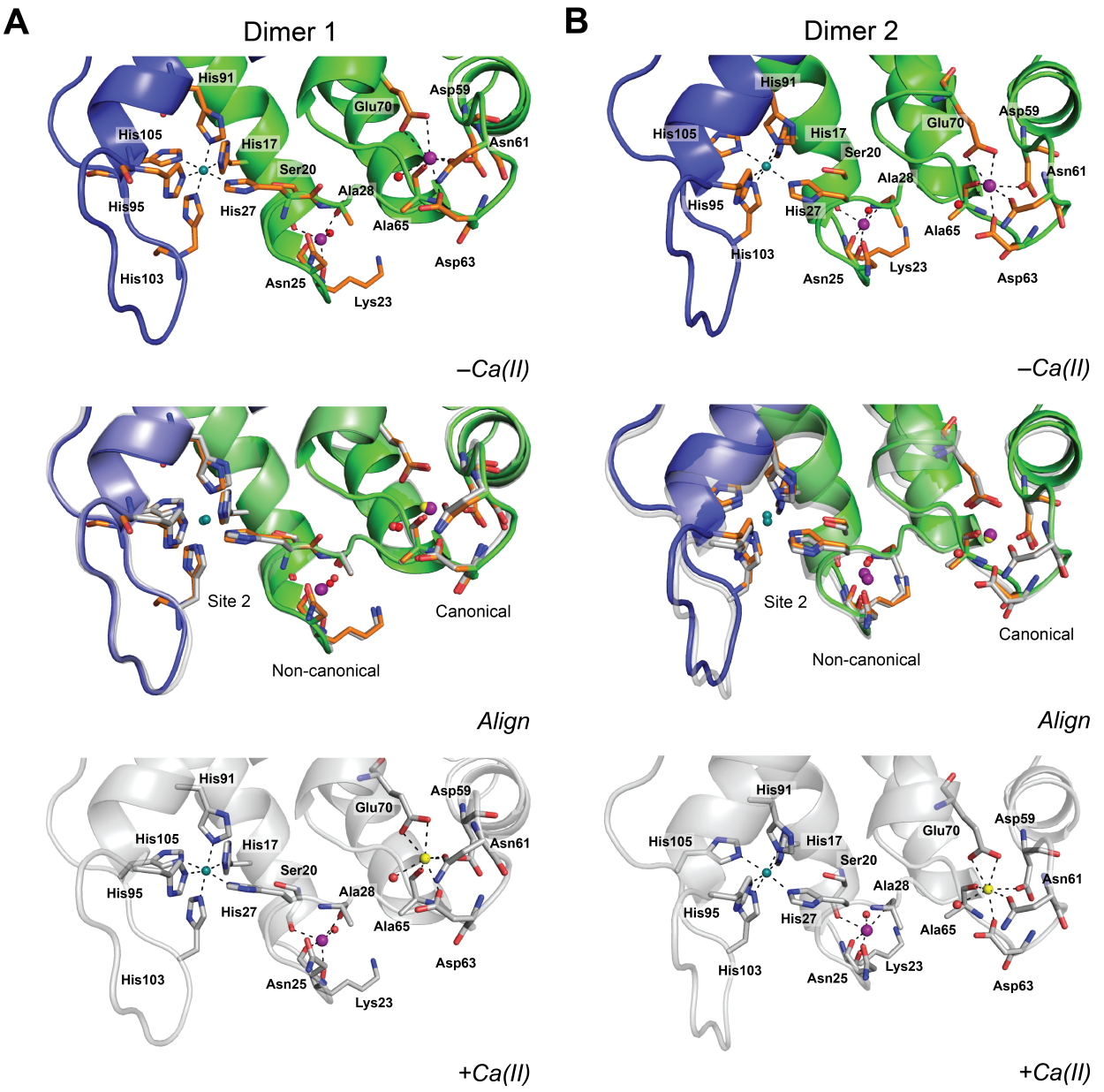

Figure S2. Structural alignment of site 2 and the S100A8 EF-hand domains. (A) Dimer 1. (B) Dimer 2. The Ca(II)-free structure is in color (top panels), and the Ca(II)-bound structure is in gray (bottom panels). The residues of site 2 and the EF-hand domains are depicted as orange (–Ca(II)) or gray (+Ca(II)) sticks. Little conformational change between the structures is observed in the structural alignment (middle panels). The metal–ligand bonds are shown as dashed lines. S100A8 is green. S100A9 is blue. Ni(II) ions are depicted as teal spheres. Water molecules are depicted as red spheres.

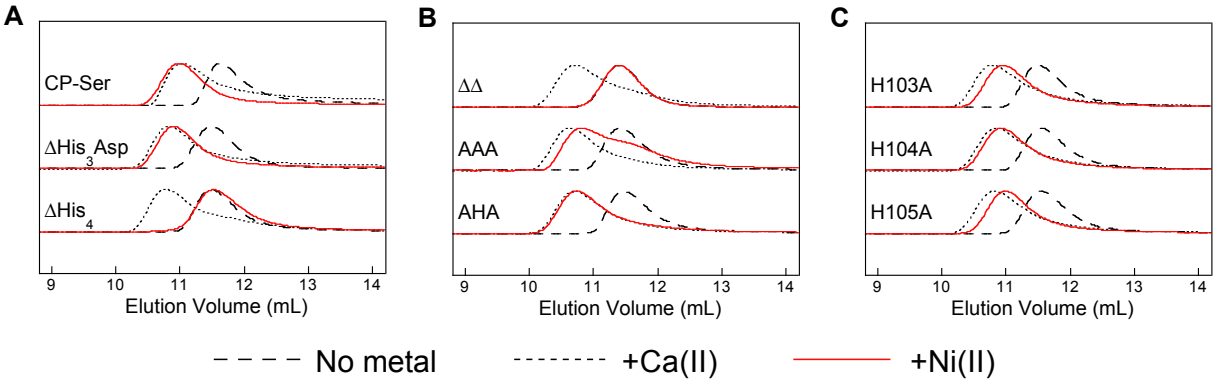

Figure S3. Ni(II) coordination at site 2 causes heterotetramerization. The analytical SEC chromatograms of (A) CP-Ser, ΔHis$_3$Asp, ΔHis$_4$, (B) ΔΔ, AAA, AHA, (C) H103A, H104A, and H105A in 75 mM HEPES, 100 mM NaCl, pH 7.0 are presented (30 μM protein). The +Ni(II) samples contained 5 equiv of Ni(II), and the +Ca(II) samples were analyzed in running buffer containing 2 mM Ca(II). The chromatograms were normalized to maximum peak heights of 1.

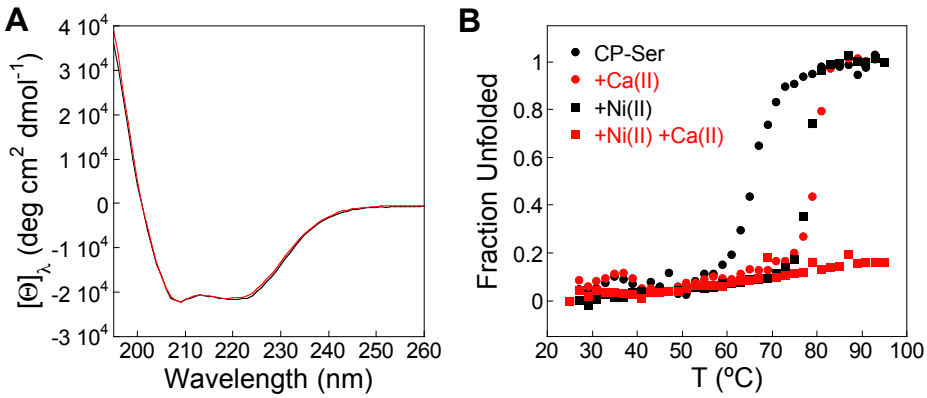

Figure S4. Circular dichroism spectra and thermal denaturation of Ni(II)-bound CP-Ser. (A) Circular dichroism (CD) spectra of 10 μM CP-Ser in presence of 5 equiv Ni(II) in the absence (black line) and presence (red line) of 2 mM Ca(II)) in 1 mM Tris-HCl, pH 7.5 at room temperature. (B) Thermal denaturation curves of 10 μM CP-Ser in 1 mM Tris-HCl, pH 7.5 in the absence and presence of 5 equiv Ni(II) and/or 2 mM Ca(II). Three independent thermal scans were conducted, and the mean value of fraction unfolded protein, calculated by ellipticity at 222 nm, is reported (*n* = 3).

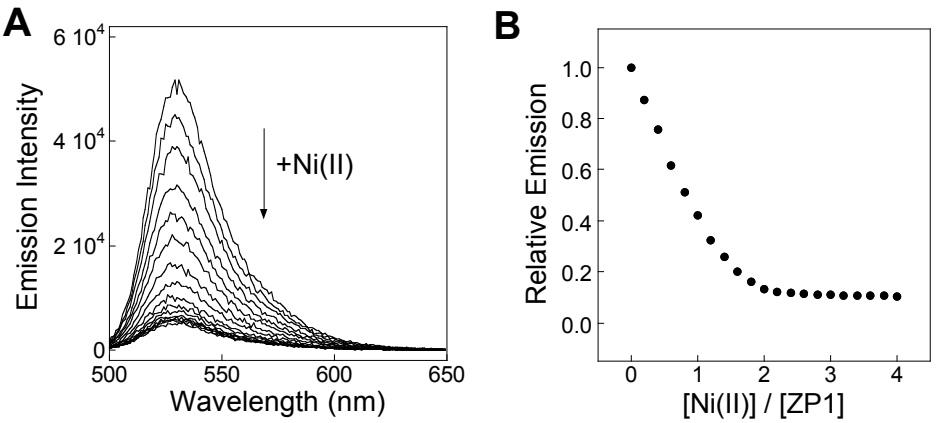

Figure S5. Direct titration of Zinpyr-1 (ZP1) with Ni(II). (A) Emission spectra of 1 μM ZP1 titration with Ni(II) (0–4 μM). (B) The normalized integrated emission of 1 μM ZP1 plotted against equivalents of Ni(II). ZP1 coordinates two equivalents of Ni(II). The buffer was 75 mM HEPES, 100 mM NaCl, pH 7.0, and the data were collected at 25 ºC.

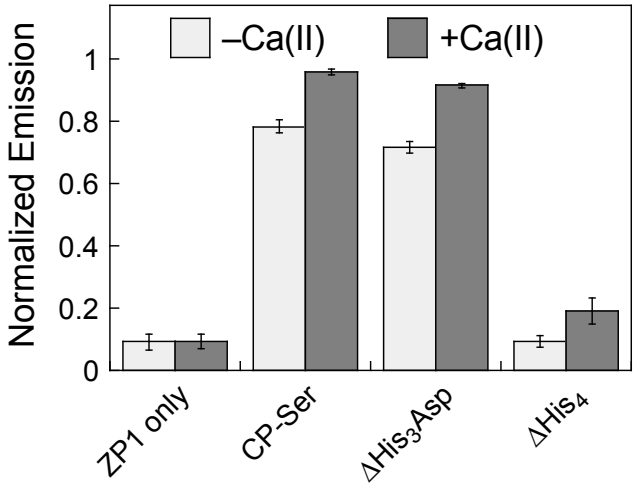

Figure S6. ZP1 Ni(II) competition with CP-Ser. Emission response of 1 μM ZP1, 2 μM Ni(II), and 4 μM CP in the absence (light gray bars) and presence (dark gray bars) of 200 μM Ca(II). The integrated emission was normalized to that of the Ni(II)-free solution after 20-h incubation. The buffer was 75 mM HEPES, 100 mM NaCl, pH 7.0, and the data were collected at 25 ºC. The mean ± SDM is reported (*n* = 3).

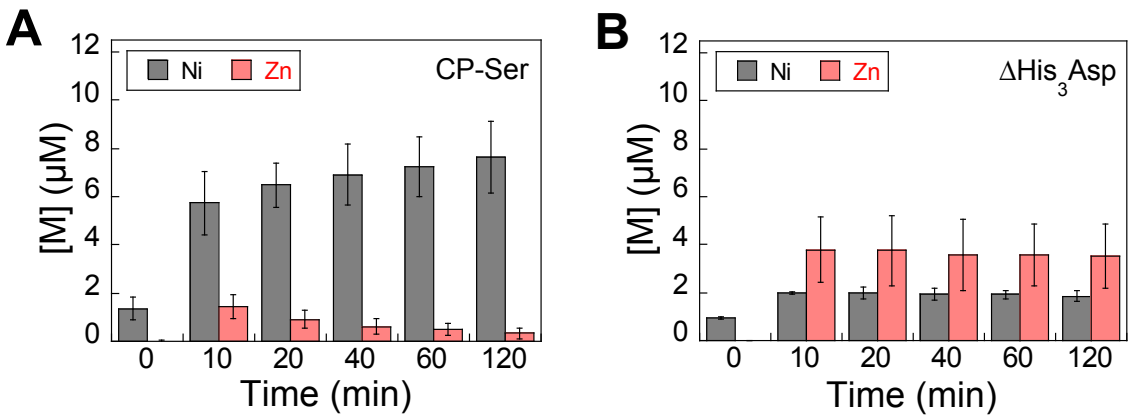

Figure S7. Metal substitution at the His_3Asp site (site 1) in the absence of Ca(II). (A) Metal content of filtrate of CP-Ser (10 μM) pre-incubated with 20 μM Ni(II) and supplemented with 10 μM Zn(II). (B) Metal content of filtrate of ΔHis_3Asp (10 μM) pre-incubated with 10 μM Ni(II) and supplemented with 10 μM Zn(II). This experiment was compromised because the results show ca. 4 μM Zn(II) in the fitrate, indicating that non-specific metal binding occurred for ΔHis_3Asp in the absence of Ca(II) ions under these conditions. All protein/metal solutions were prepared in 75 mM HEPES, 100 mM NaCl, pH 7.0. Protein was incubated for 1 h with Ni(II) before Zn(II) addition. The t = 0 h time point is the filtrate before Zn(II) addition, and all subsequent times correspond to the time post-Zn(II) addition. The Ni (black) and Zn (red) concentrations were measured by ICP-MS. The mean and SDM are reported (*n* = 3).

Caption for Supporting Video

Supporting Video. Conformational changes at site 1 and the EF-hand domains associated with Ca(II) and Ni(II) binding. The first crystal structure that is shown is dimer 1 in the presence of Ni(II) and in the absence of Ca(II) (time: 00:00 to 00:06). The second crystal structure is dimer 1 in the presence of Ni(II) and Ca(II) (PDB: 5W1F) (time: 00:10 to 00:16). The third crystal structure is dimer 2 in the presence of Ni(II) and Ca(II) (PDB: 5W1F) (time: 00:20 to 00:26). This schematic representation shows that Ca(II) binding at the canonical EF-hand domain helps to position the His_3Asp motif at site 1. The Ca(II)-free structure is depicted in color, where S100A8 is green and S100A9 is blue. The Ca(II)-bound structures are in gray. The residues of site 1 and the EF-hand domains are in orange (–Ca(II)) or gray (+Ca(II)). Ni(II) ions are teal spheres. Na(I) ions are purple spheres. Ca(II) ions are yellow spheres. Water molecules are red spheres.

Supporting References

(1) Walkup, G. K.; Burdette, S. C.; Lippard, S. J.; Tsien, R. Y. A new cell-permeable fluorescent probe for Zn^{2+}. *J. Am. Chem. Soc.* **2000**, *122*, 5644–5645.

(2) Brophy, M. B.; Hayden, J. A.; Nolan, E. M. Calcium ion gradients modulate the zinc affinity and antibacterial activity of human calprotectin. *J. Am. Chem. Soc.* **2012**, *134*, 18089–18100.

(3) Brophy, M. B.; Nakashige, T. G.; Gaillard, A.; Nolan, E. M. Contributions of the S100A9 C-terminal tail to high-affinity Mn(II) chelation by the host-defense protein human calprotectin. *J. Am. Chem. Soc.* **2013**, *135*, 17804–17817.

(4) Nakashige, T. G.; Zygiel, E. M.; Drennan, C. L.; Nolan, E. M. Nickel sequestration by the host-defense protein human calprotectin. *J. Am. Chem. Soc.* **2017**, *139*, 8828–8836.

(5) R Core Team. *R: A Language and Environment for Statistical Computing* (R Core Team, Vienna, Austria, 2013).

(6) Morin, A.; Eisenbraun, B.; Key, J.; Sanschagrin, P. C.; Timony, M. A.; Ottaviano, M.; Sliz, P. Collaboration gets the most out of software. *eLife* **2013**, *2*, e01456.

(7) Otwinowski, Z.; Minor, W., Processing of X-ray diffraction data collected in oscillation mode. In *Methods Enzymol.*, Academic Press: 1997; Vol. Volume 276, pp 307–326.

(8) Gagnon, D. M.; Brophy, M. B.; Bowman, S. E. J.; Stich, T. A.; Drennan, C. L.; Britt, R. D.; Nolan, E. M. Manganese binding properties of human calprotectin under conditions of high and low calcium: X-ray crystallographic and advanced electron paramagnetic resonance spectroscopic analysis. *J. Am. Chem. Soc.* **2015**, *137*, 3004–3016.

(9) McCoy, A. J.; Grosse-Kunstleve, R. W.; Adams, P. D.; Winn, M. D.; Storoni, L. C.; Read, R. J. *Phaser* crystallographic software. *J. Appl. Crystallogr.* **2007**, *40*, 658–674.

(10) Adams, P. D.; Grosse-Kunstleve, R. W.; Hung, L.-W.; Ioerger, T. R.; McCoy, A. J.; Moriarty, N. W.; Read, R. J.; Sacchettini, J. C.; Sauter, N. K.; Terwilliger, T. C. *PHENIX:*

building new software for automated crystallographic structure determination. Acta *Crystallogr. Sect. D: Biol. Crystallogr.* **2002**, *58*, 1948–1954.

(11) Emsley, P.; Lohkamp, B.; Scott, W. G.; Cowtan, K. Features and development of *Coot*. *Acta Crystallogr. Sect. D: Biol. Crystallogr.* **2010**, *66*, 486–501.

(12) Lebrette, H.; Borezee-Durant, E.; Martin, L.; Richaud, P.; Boeri Erba, E.; Cavazza, C. Novel insights into nickel importat in *Staphylococcus aureus*: the positive role of free histidine and structural characterization of a new thiazolidine-type nickel chelator. *Metallomics* **2015**, *7*, 613–621.

(13) Ermler, U.; Grabarse, W.; Shima, S.; Goubeaud, M.; Thauer, R. K.Crystal structure of methyl-coenzyme M reductase: the key enzyme of biological methane formation. *Science* **1997**, *278*, 1457–1462.

(14) Pochapsky, T. C.; Pochapsky, S. S.; Ju, T.; Hoefler, C.; Liang, J. A refined model for the structure of acireductone dioxygenase from *Klebsiella* ATCC 8724 incorporating residual dipolar couplings. *J. Biomol. NMR* **2006**, *34*, 117–127.

(15) He, M. M.; Clugston, S. L.; Honek, J. F.; Matthews, B. W. Determination of the structure of *Eschierchia coli* glyoxalase I suggests a structural basis for differential metal activation. *Biochemistry* **2000**, *39*, 8719–8727.

(16) Weekes, D.; Miller, M. D.; Krishna, S. S.; McMullan, D.; McPhillips, T. M.; Acosta, C.; Canaves, J. M.; Elsliger, M.-A.; Floyd, R.; Grzechnik, S. K.; Jaroszewski, L.; Klock, H. E.; Koesema, E.; Kovarik, J. S.; Kreusch, A.; Morse, A. T.; Quijano, K.; Spraggon, G.; van den Bedem, H.; Wolf, G.; Hodgson, K. O.; Wooley, J.; Deacon, A. M.; Godzik, A.; Lesley, S. A.; Wilson, I. A. Crystal structure of a transcription regulator (TM1602) from *Thermotoga maritima* at 2.3 Å resolution. *Proteins: Struct., Funct., Bioinf.* **2007**, *67*, 247–252.

(17) Gomis-Rüth, F.; Grams, F.; Yiallouros, I.; Nar, H.; Küsthardt, U.; Zwilling, R.; Bode, W.; Stöcker, W. Crystal structures, spectroscopic features, and catalytic properties of cobalt(II), copper(II), nickel(II), and mercury(II) derivatives of the zinc endopeptidase

astacin. A correlation of structure and proteolytic activity. *J. Biol. Chem.* **1994**, *269*, 17111–17117.

(18) Kishishita, S. i.; Okajima, T.; Kim, M.; Yamaguchi, H.; Hirota, S.; Suzuki, S.; Kuroda, S. i.; Tanizawa, K.; Mure, M. Role of copper ion in bacterial copper amine oxidase: spectroscopic and crystallographic stuides of metal-substituted enzymes. *J. Am. Chem. Soc.* **2003**, *125*, 1041–1055.

(19) Swan, M. K.; Solomons, J. T. G.; Beeson, C. C.; Hansen, T.; Schönheit, P.; Davies, C. Strong evidence for a hydride transfer mechanism of catalysis in phosphoglucose isomerase from *Pyrococcus furiosus*. *J. Biol. Chem.* **2003**, *278*, 47261–47268.

(20) de las Rivas, B.; Fox, G. C.; Angulo, I.; Ripoll, M. M.; Rodríguez, H.; Muñoz, R.; Mancheño, J. M. Crystal structure of the hexameric catabolic ornithine transcarboamylase from *Lactobacillus hilgardii*: structural insights into the oligomeric assembly and metal binding. *J. Mol. Biol.* **2009**, *393*, 425–434.

(21) Rajan, S. S.; Yang, X.; Shuvalova, L.; Collart, F.; Anderson, W. F. YfiT from *Bacillus subtilis* is a probable metal-dependent hydrolase with an unusual four-helix bundle topology. *Biochemistry* **2004**, *43*, 15472–15479.

(22) Pearson, M. A.; Michel, L. O.; Hausinger, R. P.; Karplus, P. A. Structures of Cys319 variants and acetohydroxamate-inhibited *Klebsiella aerogenes* urease. *Biochemistry* **1997**, *36*, 8164–8172.

(23) Shi, R.; Munger, C.; Asinas, A.; Benoit, S. L.; Miller, E.; Matte, A.; Maier, R. J.; Cygler, M. Crystal structures of apo and metal-bound forms of the UreE protein from *Helicobacter pylori*: role of multiple metal binding sites. *Biochemistry* **2010**, *49*, 7080–7088.

(24) Barondeau, D. P.; Kassmann, C. J.; Bruns, C. K.; Tainer, J. A.; Getzoff, E. D.Nickel superoxide dismutase structure and mechanism. *Biochemistry* **2004**, *43*, 8038–8047.

(25) Volbeda, A.; Martin, L.; Cavazza, C.; Matho, M.; Faber, B. W.; Roseboom, W.; Albracht, S. P. J.; Garcin, E.; Rousset, M.; Fontecilla-Camps, J. C. Structural differences between

the ready and unready oxidized states of [NiFe] hydrogenases. *J. Biol. Inorg. Chem.* **2005**, *10*, 239–249.

(26) Schreiter, E. R.; Wang, S. C.; Zamble, D. B.; Drennan, C. L. NikR-operator complex structure and the mechanism of repressor activation by metal ions. *Proc. Natl. Acad. Sci. U.S.A.* **2006**, *103*, 13676–13681.

(27) Desguin, B.; Zhang, T.; Soumillion, P.; Hols, P.; Hu, J.; Hausinger, R. P. Metalloproteins: a tethered niacin-derived pincer complex with a nicek-carbon bond in lactate racemase. *Science* **2015**, *349*, 66–69.

(28) Brinen, L. S.; Willett, W. S.; Craik, C. S.; Fletterick, R. J. X-ray structures of a designed binding site in trypsin show metal-dependent geometry. *Biochemistry* **1996**, *35*, 5999–6009.

(29) Doudeva, L. G.; Huang, H.; Hsia, K.-C.; Shi, Z.; Li, C.-L.; Shen, Y.; Cheng, Y.-S.; Yuan, H. S. Crystal structure analysis and metal-dependent stability and activity studies of the ColE7 endonuclease domain in complex with DNA/Zn^{2+} or inhibitor/Ni^{2+}. *Protein Science* **2006**, *15*, 269–280.

(30) Schreiter, E. R.; Sintchak, M. D.; Guo, Y.; Chivers, P. T.; Sauer, R. T.; Drennan, C. L. Crystal structure of the nickel-responsive transcription factor NikR. *Nat. Struct. Biol.* **2003**, *10*, 794–799.